Chapter 8
Atmosphere-Water Exchange

Bernd Jähne

Glossary

Bulk coefficients	c_i relate the *transfer velocity* k for a species i to the *wind velocity* U_r in a reference height, typically at 10 m above the mean water level: $c_i = k_i/U_r$. From the bulk coefficient, the flux density j_i of a species can be computed as $j_i = c_i(C_r - C_0)U_r$, where C_r and C_0 are the corresponding concentrations at the reference height and right at the water surface, respectively. For momentum density (ρU) the bulk coefficients is also known as the *drag coefficient* c_D. It can also be expressed as $c_D = (u_*/U_r)^2$ with the momentum flux given by $j_m = \rho u_*^2$; u_* is the *friction velocity*.
Friction velocity	u_* is a measure for the tangential force per area applied by the wind at the water surface, the shear stress $\tau = \rho u_*^2$, which is also equal to the vertical momentum flux density j_m.
Mass boundary layer	Thickness of the layers at both sides of the water surface in which transport of mass by turbulence is smaller than by molecular diffusion.

This chapter was originally published as part of the Encyclopedia of Sustainability Science and Technology edited by Robert A. Meyers. DOI:10.1007/978-1-4419-0851-3

B. Jähne (✉)
Institute for Environmental Physics and Heidelberg Collaboratory
for Image Processing (HCI), University of Heidelberg, Speyerer Straße 6,
69115 Heidelberg, Germany
e-mail: Bernd.Jaehne@iwr.uni-heidelberg.de

J.S. Gulliver (ed.), *Transport and Fate of Chemicals in the Environment: Selected Entries from the Encyclopedia of Sustainability Science and Technology*,
DOI 10.1007/978-1-4614-5731-2_8,

Schmidt and Prandtl numbers, Sc and Pr	The Schmidt and Prandtl numbers are the ratio of kinematic viscosity ν (molecular diffusion coefficient for momentum) and the molecular diffusion coefficients for the corresponding chemical species, D, and heat, D_h, respectively. Thus, these numbers express how much slower chemical species and heat, respectively, are transported by molecular processes than momentum. In air, these numbers are in the order of one; in water, the Prandtl number is about 10 and the Schmidt number about 1,000.
Transfer velocity	k is the velocity by which a momentum, heat, and chemical are transported across the surface; because of the concentration discontinuity at the water surface, the transfer velocity on the air side is different from the transfer velocity on the water side.
Viscous boundary layer	Thickness of the layers at both sides of the water surface in which transport of momentum by turbulent is smaller than by molecular friction, resulting in a linear velocity profile in this layer.

Definition of the Subject

Gaseous and volatile chemical species reside not only in the atmosphere. Because they dissolve in water, they are also distributed in the hydrosphere. The by far largest part of the hydrosphere is the ocean. Therefore, the exchange between atmosphere and oceans is the most important process for the fate of gaseous and volatile chemical species (Table 8.1).

For long-lived species, that is, life time by reaction larger than residence times in either the atmosphere or the ocean, two basic factors determine the fate of these species. For time scales longer than the turnover time of ocean mixing, which is much slower than the same process in the atmosphere, the solubility of the species determines where it ends up. On much shorter time scales, the speed by which the species are exchanged between atmosphere and ocean and the concentration difference determines the flux between these two compartments.

While turbulent mixing is quite fast within the ocean and the atmosphere, it becomes more and more inefficient, the closer a species is transported to the surface. The final step toward the interface must be overcome by molecular diffusion, which is a slow process, especially in water. Therefore, very thin mass boundary layers at both sides of the water surface, in which turbulent transport is

Table 8.1 Comparison of size (as depth in m over entire earth surface) and mass of atmosphere and global water storage

System	Depth (m)	Mass (10^{18} kg)
Oceans	2,624	1,382
Ice caps and glaciers	47	25
Total ground water	46	24
Lakes	0.35	0.18
Rivers	0.004	0.002
Atmosphere	8,000	5.3

slower than molecular transport, are the bottleneck of the exchange between atmosphere and ocean.

In this way, tiny layers only about 20–200 μm thick in the water and 200–2,000 μm thick in the air control the exchange process. In consequence, the crucial question is which processes determine the thickness of these layers.

Introduction

Research in air–water gas exchange dates back more than a century. Bohr [1], for example, was one of the first to study the exchange of carbon dioxide in a stirred bottle. With the early observation of increasing carbon dioxide concentration in the atmosphere interest in air-sea gas exchange rose considerably, triggered by the question how much of the excess carbon dioxide would go into the ocean [2, 3]. Since then significant and continuous research work was devoted for a better understanding of air–water mass exchange, but the mechanisms of the exchange processes are still not fully understood even today.

This entry is divided into three major parts and partly based on previous reviews of the author on the same subject [4–6]. Section "Mechanisms of Atmosphere–Water Exchange" describes the basic mechanisms of air–water exchange and the many parameters influencing it. Focusing on field data, section "Experimental Techniques and Results" summarizes the various experimental techniques and gives a synthesis of the available experimental data. Using the information collected in the previous two sections, section "Empiric Parametrization" tries to give the best possible empirical parametrization of the exchange rate and section "Future Directions" points to future directions of research.

Mechanisms of Atmosphere–Water Exchange

Turbulent and Molecular Transport

The transfer of gases and volatile chemical species between the atmosphere and oceans is driven by a concentration difference and the transport by molecular

and turbulent motion. Both types of transport processes can be characterized by *diffusion coefficients*, denoted by D and K_c, respectively. The resulting flux area density $\boldsymbol{j}_c$ is proportional to the diffusion coefficient and the concentration gradient:

$$j_c = -(D+K_c(z))\nabla_c. \tag{8.1}$$

In a stationary homogeneous case and without sinks and sources by chemical reactions, the flux density $\boldsymbol{j}$ is in vertical direction and constant. Then integration of Eq. 8.1 yields vertical concentration profiles:

$$C(z_r) - C(0) = j_c \int_0^{z_r} \frac{1}{D + K_c(z)} dz. \tag{8.2}$$

The molecular diffusion coefficient is proportional to the velocity of the molecules and the free length between collisions. The same concept can be applied to turbulent diffusion coefficients. Far away from the interface, the free length (called *mixing length*) is set proportional to the distance from the interface and the turbulent diffusion coefficient K_c for mass transfer is:

$$K_c = \frac{k}{Sc_t} u_* z, \tag{8.3}$$

where $\kappa = 0.41$ is the *von Kármán constant*, u_*, the *friction velocity*, a measure for the velocity fluctuations in a turbulent flow, and $Sc_t = K_m/K_c$ the *turbulent Schmidt number*. Closer to the interface, the turbulent diffusion coefficients are decreasing even faster. Once a critical length scale l is reached, the Reynolds number $Re = u_* l/\nu$ (ν is the kinematic viscosity, the molecular diffusion coefficient for momentum) becomes small enough so that turbulent motion is attenuated by viscosity. The degree of attenuation depends on the properties of the interface. At a smooth solid wall, $K_c \propto z^3$, at a free water interface it could be in the range between $K_c \propto z^3$ and $K_c \propto z^2$ depending on surface conditions.

Viscous and Mass Boundary Layers

Boundary layers are formed on both sides of the interface (Fig. 8.1). When the turbulent diffusivity becomes equal to the kinematic viscosity, the edge of the *viscous boundary layer* is reached. As the name implies, this layer is dominated by viscous dissipation and the velocity profile becomes linear because of a constant diffusivity. The edge of the *mass boundary layer* is reached when the turbulent diffusivity becomes equal to the molecular diffusivity. The relative thickness of both boundary layers depends on the dimensionless ratio $Sc = \nu/D$ (*Schmidt number*).

The viscous and mass boundary layers are of about the same thickness in the air, because values of D for various gaseous species and momentum are about the same (Sc_{air} is 0.56 for H_2O, 0.63 for heat, and 0.83 for CO_2). In the liquid phase, the situation is completely different. With Schmidt numbers in the range from 100 to 3,000 (Fig. 8.2, Table 8.3), molecular diffusion for a dissolved volatile chemical species is two to three orders of magnitude slower than diffusion of momentum (Table 8.2). Thus, the mass boundary layer is significantly thinner than the viscous boundary layer in the liquid phase. This means that the transfer of gases is much slower and almost entirely controlled by the tiny residual turbulence in the small top fraction of the viscous boundary layer. This basic fact makes it difficult to investigate the mechanism of air–water gas transfer both theoretically and experimentally. In addition, the transfer process depends strongly on the water temperature because the Schmidt number decreases by about a factor of 6 from 0°C to 35°C (Fig. 8.2, Table 8.3).

Description of Transport

The amount of species exchanged between the air and water across the interface can be described by a quantity with the units of a velocity. It represents the velocity with which a tracer is pushed by an imaginary piston across the surface. This quantity is known as the *transfer velocity* k (also known as the *piston velocity*, *gas exchange rate* or *transfer coefficient*). It is defined as the flux density divided by the concentration difference between the surface and the bulk at some reference level z_r:

$$k = \frac{j_c}{C_s - C_b}. \tag{8.4}$$

The inverse of the transfer velocity is known as the *transfer resistance* R:

$$R = \frac{C_s - C_b}{j_c}. \tag{8.5}$$

The indices s and b denote the surface and bulk. Both quantities can directly be related to vertical concentration profiles by introducing Eqs. 8.4 and 8.5 into Eq. 8.2:

$$R = \frac{1}{k} = \int_0^{z_r} \frac{1}{D + K_e(z)} dz. \tag{8.6}$$

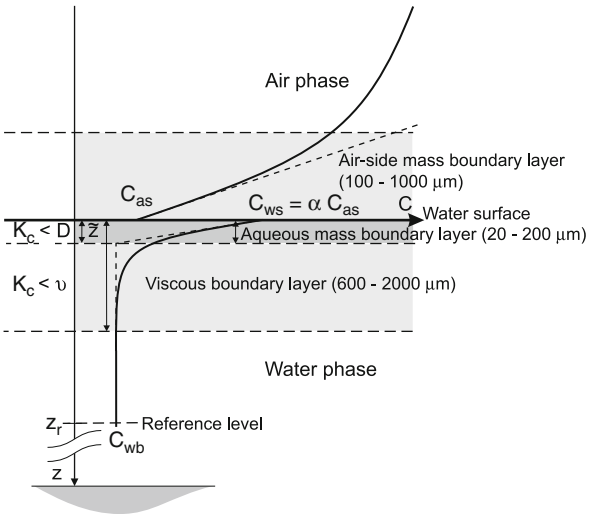

Fig. 8.1 Schematic graph of the mass boundary layers at a gas–liquid interface for a tracer with a solubility $\alpha = 3$

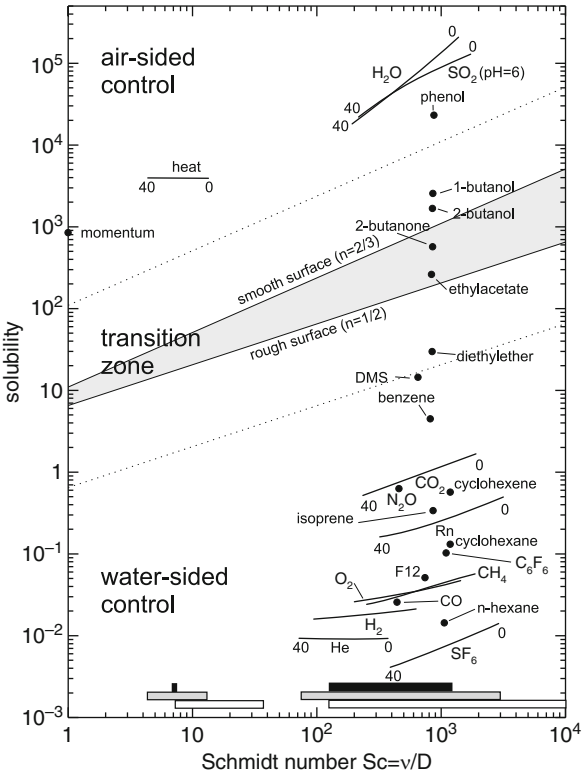

Fig. 8.2 Schmidt number/solubility diagram including various volatile tracers, momentum, and heat for a temperature range (C) as indicated. *Filled circles* refer to only a temperature of 20°C. The regions for air-side, mixed, and water-side control of the transfer process between gas and liquid phase are marked. At the solid lines, the transfer resistance is equal in both phases. The following dimensional transfer resistances were used: $r_a = 31$, $r_w = 12Sc^{2/3}$ (smooth), $r_w = 6.5Sc^{1/2}$ (wavy surface) with $r_a = R_a u_{*a}$ and $r_w = R_w u_{*w}$ (Adapted from Jähne and Haußecker [6])

Table 8.3 Schmidt numbers of various gases and volatile species in the temperature range from 0°C to 40°C

	Schmidt number								
Species	0°C	5°C	10°C	15°C	20°C	25°C	30°C	35°C	40°C
Heat	13.45	11.19	9.46	8.10	7.02	6.14	5.42	4.82	4.32
^{3}He	329	254	200	160	130	107	88	74	63
^{4}He	379	293	230	184	149	122	102	85	72
$^{4}He^{a}$	411	319	252	201	164	135	112	94	79
Ne	768	579	445	347	276	221	180	148	122
Kr	2,045	1,478	1,090	819	625	483	379	301	241
Xe	2,701	1,930	1,409	1,047	791	606	471	370	294
^{222}Rn	3,168	2,235	1,611	1,182	883	669	514	400	314
H_2	633	473	360	278	219	174	140	114	94
H_2^{a}	663	502	387	304	242	195	159	131	109
CH_4	1,908	1,400	1,047	797	616	483	383	308	250
CO_2	1,922	1,397	1,036	782	600	466	367	293	236
DMS	2,593	1,905	1,428	1,089	844	662	527	423	344
CH_3Br	2,120	1,545	1,150	870	669	522	412	329	266
F_{12} (CCl_2F_2)	3,639	2,624	1,931	1,447	1,102	851	666	527	422
F_{11}(CCl_3F)	3,521	2,549	1,883	1,416	1,082	839	658	523	420
SF_6	3,033	2,208	1,640	1,239	952	741	585	467	376

[a]In sea water

Thus, the transfer resistances over several height intervals can be added in the same way as electrical resistances that are connected in series. Typical values of the transfer velocity across the water-side mass boundary layer are 10^{-6}–10^{-5} m/s (1–10 m/day). With respect to typical mixed layer depths in the ocean of about 100 m, gas transfer is a very slow process. It takes a time constant $\tau = h/k$ = 10–100 days for the concentration of dissolved gases in the mixed layer to come into equilibrium with the atmosphere.

Boundary Layer Thickness

The *boundary layer thickness* $\tilde{z}$ is defined as the thickness of a fictional layer in which the flux is maintained only by molecular transport: $j = D(C_s - C_b)/\tilde{z}$. Then with Eq. 8.4 the boundary layer thickness is given by:

$$\tilde{z} = \frac{D}{k}. \tag{8.7}$$

Geometrically, $\tilde{z}$ is given as the intercept of the tangent to the concentration profile at the surface and the bulk (Fig. 8.1). With thicknesses between 20 and 200 μm, the mass boundary layer is extremely thin.

Table 8.2 Diffusion coefficients for various gases and volatile chemical species in deionized water and in some cases in sea water collected from Jähne et al. [18] and King et al. [20]. Die data for momentum (kinematic viscosity) are from Sündermann [22]. Column 3 and 4 contain the parameters for the fit of the diffusion coefficient: $D = A \exp[-E_a/(RT)]$, the last four columns the diffusion coefficients for 5°C, 15°C, 25°C, and 35°C

Species	Molecular mass	A (10^{-5} cm^2/s)	E_a (kJ/mole)	σ(Fit) %	Diffusion coefficient (10^{-5} cm^2/s) 5°C	15°C	25°C	35°C
Momentum	–				1,517	1,139	893.4	724.3
Momentum[a]	–				1,560	1,182	934.5	763.9
Heat	–	379.2	2.375		135.80	140.72	145.48	150.08
^{3}He[b,c]	3.02	941	11.70	2.1	5.97	7.12	8.39	9.77
^{4}He	4.00	818	11.70	2.1	5.10	6.30	7.22	8.48
^{4}He[a]		886	12.02	1.8	4.86	5.88	7.02	8.03
Ne	20.18	1,608	14.84	3.5	2.61	3.28	4.16	4.82
Kr	83.80	6,393	20.20	1.6	1.02	1.41	1.84	2.40
Xe	131.30	9,007	21.61	3.5	0.77	1.12	1.47	1.94
^{222}Rn[b]	222.00	15,877	23.26	11	0.68	0.96	1.34	1.81
H_2	2.02	3,338	16.06	1.6	3.17	4.10	5.13	6.23
H_2[a]		1,981	14.93	4.3	3.05	3.97	4.91	5.70
CH_4	16.04	3,047	18.36	2.7	1.12	1.48	1.84	2.43
CO_2	44.01	5,019	19.51	1.3	1.07	1.45	1.91	2.43
DMS[b]	62.13	2,000	18.10		0.80	1.05	1.35	1.71
CH_3Br[b]	94.94	3,800	19.10		0.98	1.31	1.71	2.20
F_{12}[b] (CCl_2F_2)	120.91	4,100	20.50		0.58	0.79	1.05	1.37
F_{11}[b](CCl_3F)	137.37	3,400	20.00		0.60	0.81	1.07	1.38
SF_6[b]	146.05	2,900	19.30		0.69	0.92	1.20	1.55

[a]In sea water
[b]Values of diffusion coefficients from fit, not measured values
[c]Set 15% higher than ^{4}He

Boundary Layer Time Constant

The *time constant* $\tilde{t}$ for the transport across the mass boundary layer is given by:

$$\tilde{t} = \frac{\tilde{z}}{k} = \frac{D}{k^2}. \tag{8.8}$$

Typical values for $\tilde{t}$ are 0.04–4 s. Any chemical reaction with a time constant larger than $\tilde{t}$ does not significantly affect the transfer process. Therefore, CO_2 can be regarded as an inert gas, but not fast hydrating acid gases such as SO_2.

The definitions of the three parameters k, $\tilde{z}$, $\tilde{t}$ are generally valid and do not depend on any models of the boundary layer turbulence. According to Eqs. 8.7 and 8.8, they are coupled via the molecular diffusion coefficient. Therefore, only one of them needs to be measured to get knowledge of all three parameters provided the molecular diffusion coefficient of the species is known.

Partitioning of Transfer Between Air and Water

Because a mass boundary layer exists on both sides, it is important to determine which one controls the transfer, that is, exhibits the largest transfer resistance (or lowest transfer velocity). At the surface itself, the thermodynamic solubility equilibrium is assumed to be established between the tracer concentrations c_a in the gas phase and c_w in the liquid phase:

$$C_{ws} = \alpha C_{as}, \tag{8.9}$$

where α is the dimensionless solubility (partition coefficient). A solubility $\alpha \neq 1$ causes a concentration jump at the surface (Fig. 8.1). Thus, the resulting total transfer velocity k_t or transfer resistance R_t can either be viewed from the gas phase or the liquid phase. Adding them up, the factor α must be considered to conserve the continuity of the concentration profile:

$$\text{air side: } \frac{1}{k_{at}} = \frac{1}{k_a} + \frac{1}{\alpha k_w}, \quad R_{at} = R_a + R_w/\alpha, \tag{8.10}$$

$$\text{water side: } \frac{1}{k_{wt}} = \frac{\alpha}{k_a} + \frac{1}{k_w}, \quad R_{wt} = \alpha R_a + R_w.$$

The total transfer velocities in air and water differ by the factor α: $k_{at} = \alpha k_{wt}$. The ratio $\alpha k_w/k_a$ determines which boundary layer controls the transfer process. A high solubility shifts control of the transfer process to the gas-phase boundary layer, and a low solubility to the aqueous layer. The solubility value for a transition from air-sided to water-sided control depends on the ratio of the transfer velocities. Typically k_w is about 100–1,000 times smaller than k_a. Thus, the transfer of even moderately soluble volatile chemical species with solubilities up to 30 is controlled by the water side. Some environmentally important species lie in a transition zone where it is required to consider both transport processes (Fig. 8.2). The transfer of highly soluble volatile and/or chemically reactive gas is controlled by the air-side transfer process and thus analogous to the transfer of water vapor. The following considerations concentrate on the water-side transfer process.

Gas Exchange at Smooth Water Surfaces

At smooth water surfaces, the theory of mass transfer is well established because it is equivalent to mass transfer to a smooth solid wall. The turbulent diffusivity can be described by the classic approach of Reichardt [7] with an initial z^3 increase that smoothly changes to a linear increase in the turbulent layer as in Eq. 8.3.

Then integration of Eq. 8.6 yields the following approximation for Schmidt numbers higher than 100 [12, 16]:

$$k_w = u_{*w} \frac{1}{12.2} Sc^{-2/3} \quad Sc > 60. \tag{8.11}$$

This equation establishes the basic analogy between momentum transfer and gas exchange. The transfer coefficients are proportional to the friction velocity in water, which describes the shear stress (tangential force per unit area) $\tau = \rho_w u_{*w}^2$ applied by the wind field at the water surface. Assuming stress continuity at the water surface, the friction velocity in water is related to the friction velocity in air by:

$$u_{*w} = u_{*a} \left(\frac{\rho_a}{\rho_w} \right)^{1/2}. \tag{8.12}$$

The friction velocity in air, u_{*a}, can further be linked via the drag coefficient to the wind speed U_R at a reference height: $c_D = (u_{*a}/U_R)^2$. Depending on the roughness of the sea surface, the drag coefficient has values between 0.8 and $2.4 \cdot 10^{-3}$. In this way, the gas exchange rate is directly linked to the wind speed. The gas exchange further depends on the chemical species and the water temperature via the Schmidt number.

Influence of Waves

A free water surface is neither solid nor is it smooth as soon as short wind waves are generated. On a free water surface, velocity fluctuations are possible. Thus, there can be convergence or divergence zone at the surface; surface elements may be dilated or contracted. At a clean water surface, dilation or contraction of a surface element does not cause restoring forces, because surface tension only tries to minimize the total free surface area, which is not changed by this process. As a consequence of this hydrodynamic boundary condition, the turbulent diffusivity normal to the interface can now increase with the distance squared from the interface, $K_c \propto z^2$. Then:

$$k_w = u_{*w} \frac{1}{\beta} Sc^{-1/2}, \tag{8.13}$$

where β is a dimensionless constant.

In comparison to the smooth case in Eq. 8.11, the exponent n of the Schmidt number drops from $-2/3$ to $-1/2$. This increases the transfer velocity for a Schmidt number of 600 by about a factor of 3. The total enhancement depends on the value of the constant β.

Wind waves cannot be regarded as static roughness elements for the liquid flow because their characteristic particle velocity is of the same order of magnitude as

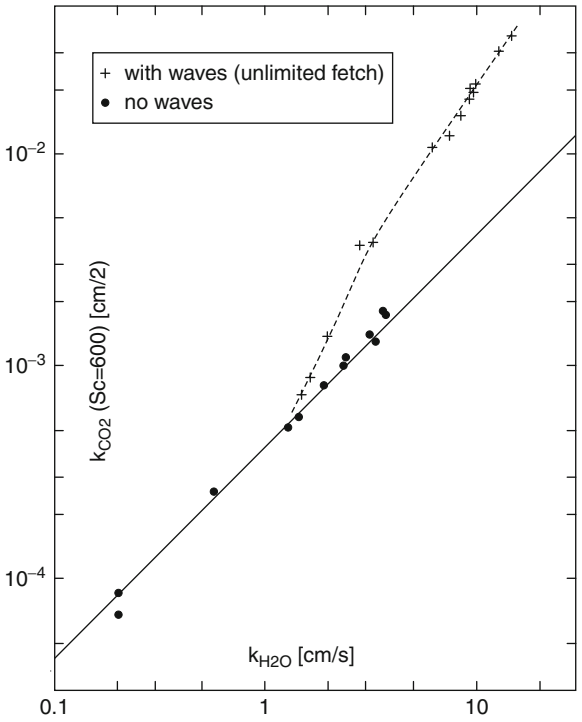

Fig. 8.3 Transfer velocity of carbon dioxide plotted against the transfer velocity of water vapor. Measurements from a small annular wind/wave facility Jähne [15]

the velocity in the shear layer at the surface. This fact causes a basic asymmetry between the turbulent processes on the air and on the water sides of the interface. Therefore, the wave effect on the turbulent transfer in the water is much stronger and of quite different character than in the air. This basic asymmetry can be seen if the transfer velocity for CO_2 is plotted against the transfer velocity for water vapor (Fig. 8.3, [15]). At a smooth water surface, the points fall well on the theoretical curve predicted by the theory for a smooth rigid wall. However, as soon as waves occur at the water surface, the transfer velocity of CO_2 increases significantly beyond the predictions.

Even at high wind speeds, the observed surface increase is well below 20% [24]. When waves are generated by wind, energy is not only transferred via shear stress into the water but a second energy cycle is established. The energy put by the turbulent wind into the wave field is transferred to other wave numbers by nonlinear wave–wave interaction and finally dissipated by wave breaking, viscous dissipation, and turbulence. The turbulent wave dissipation term is the least known term and of most importance for enhanced near-surface turbulence. Evidence for enhanced turbulence levels below wind waves has been reported from field and laboratory measurements. Experimental results also suggest that the gas transfer rate is better correlated with the *mean square slope* of the waves as an integral measure for the nonlinearity of the wind wave field than with the wind speed.

It is not yet clear, however, to what extent *microscale wave breaking* can account for the observed enhanced gas transfer rates. A gravity wave becomes instable and generates a steep train of capillary waves at its leeward face and has a turbulent wake. This phenomenon can be observed even at low wind speeds, as soon as wind waves are generated. At higher wind speeds, the frequency of microscale wave breaking increases.

At high wind speeds, wave breaking with the entrainment of bubbles may enhance gas transfer further. This phenomenon complicates the gas exchange between atmosphere and the oceans considerably [19, 26]. First, bubbles constitute an additional exchange surface. This surface is, however, only effective for gases with low solubility. For gases with high solubility, the gas bubbles quickly come into equilibrium so that a bubble takes place in the exchange only for a fraction of its life time. Thus bubble-mediated gas exchange depends – in contrast to the exchange at the free surface – on the solubility of the gas tracer. Second, bubble-mediated gas transfer shifts the equilibrium value to slight supersaturation due to the enhanced pressure in the bubbles by surface tension and hydrostatic pressure. Third, breaking waves also enhance near-surface turbulence during the breaking event and the resurfacing of submerged bubbles [17].

Experimental data are still too sparse for the size and depth distribution of bubbles and the flux of the bubbles through the interface under various sea states for a sufficiently accurate modeling of bubble-mediated air-sea gas transfer and thus a reliable estimate of the contribution of bubbles to the total gas transfer rate. Some experiments from wind/wave tunnels and the field suggest that significant enhancements can occur, other experiments could not observe a significant influence of bubbles.

Influence of Surface Films

A film on the water surface creates pressure that works against the contraction of surface elements. This is the point at which the physicochemical structure of the surface influences the structure of the near-surface turbulence as well as the generation of waves [13, 21]. As at a rigid wall, a strong film pressure at the surface maintains a two-dimensional continuity at the interface just as at a rigid wall. Therefore, Eq. 8.11 should be valid for a smooth film-covered water surface and has indeed been verified in wind/wave tunnel studies as the lower limit for the transfer velocity. As a consequence, both Eqs. 8.11 and 8.13 can only be regarded as limiting cases. A more general approach is required that has not yet been established. One possibility is a generalization of Eqs. 8.11 and 8.13 to:

$$k_w = u_{*w} \frac{1}{\beta(s)} Sc^{-n(s)}, \tag{8.14}$$

where both β and n depend on dimensionless parameters describing the surface conditions s. Even films with low film pressure may easily decrease the gas transfer rate to half of its value at clean water surface conditions. But still too few measurements at sea are available to establish the influence of surfactants on gas transfer for oceanic conditions more quantitatively.

Experimental Techniques and Results

Laboratory Facilities

Laboratory facilities play an important role in the investigation of air-sea gas transfer. Only laboratory studies allow a systematic study of the mechanisms and are thus an indispensable complement to field experiments. Almost all basic knowledge about gas transfer has been gained by laboratory experiments in the past.

Geochemical Tracer Techniques

The first oceanic gas exchange measurements were performed using geochemical tracer methods such as the ^{14}C [2], $^{3}He/T$ [23], or $^{222}Rn/^{226}Ra$ [8, 9] methods. The volume and time-average flux density is given by mass balance of the tracer concentration in a volume of water V_w:

$$V_w \dot{c}_w = F_w j \quad or \quad j = h_w \dot{c}_w, \tag{8.15}$$

where F_w, and h_w are the surface area and the effective height V_w / F_w of a well-mixed water body, respectively. The time constant $\tau_w = h_w / k$ is in the order of days to weeks. It is evident that the transfer velocities obtained in this way provide only values integrated over a large horizontal length scales and time scales in the order of τ_w. Thus a parametrization of the transfer velocity is only possible under steady state conditions over extended periods. Moreover, the mass balance contains many other sources and sinks besides air-sea gas exchange and thus may cause severe systematic errors in the estimation of the transfer velocity. Consequently, mass balance methods are only poorly suited for the study of the mechanisms of air–water gas transfer.

Tracer Injection

The pioneering lake studies for tracer injection used sulfur hexafluoride (SF_6). However, the tracer concentration decreases not only by gas exchange across the interface but also by horizontal dispersion of the tracer. This problem can be overcome by the *dual tracer technique* [10] simultaneously releasing two tracers with different diffusivities (e.g., SF_6 and ^3He). When the ratio of the gas transfer velocities of the two tracers is known, the dilution effect by tracer dispersion can be corrected, making it possible to derive gas transfer velocities. But the basic problem of mass balance techniques, that is, their low temporal resolution, remains also with artificial tracer approaches.

Eddy Correlation Flux Measurements

Eddy correlation techniques are used on a routine basis in micrometeorology, that is, for tracers controlled by the boundary layer in air (momentum, heat, and water vapor fluxes). Direct measurements of the air-sea fluxes of gas tracers are very attractive because the flux densities are measured directly and have a much better temporal resolution than the mass balance based techniques. Unfortunately, large experimental difficulties arise when this technique is applied to gas tracers controlled by the aqueous boundary layer [Broecker 1986, 14]. The concentration difference in the air is only a small fraction of the concentration difference across the aqueous mass boundary layer. But after more than 20 years of research has this technique delivered useful results. Some successful measurements under favorable conditions have been reported and it appears that remaining problems can be overcome in the near future.

Passive and Active Thermography

The basic idea of this technique is to determine the concentration difference across the mass boundary layer when the flux density j of the tracer across the interface is known. The local transfer velocity can be determined by simply measuring the concentration difference Δc across the aqueous boundary layer (cold surface skin temperature) according to Eq. 8.4 with a time constant $\tilde{t}$ for the transport across the boundary layer Eq. 8.8. This technique is known as the *controlled flux technique* (CFT).

Heat proves to be an ideal tracer for the CFT. The temperature at the water surface can then be measured with high spatial and temporal resolution using IR thermography. A known and controllable flux density can be applied by using infrared radiation. Infrared radiation is absorbed in the first few ten micrometers at the water surface. Thus a heat source is put right at top of the aqueous viscous boundary layer. Then the CFT directly measures the water-side heat transfer velocity.

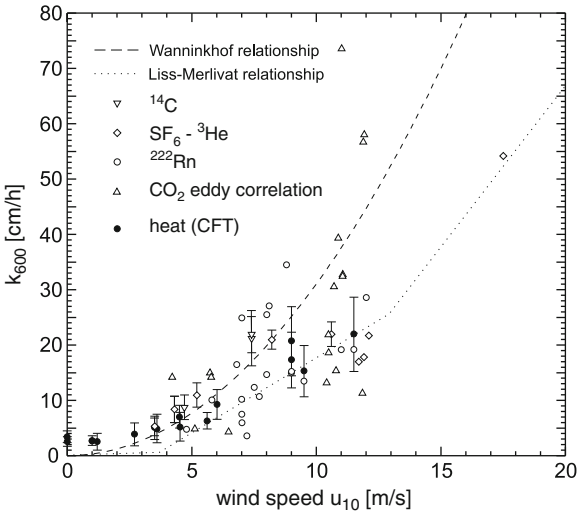

Fig. 8.4 Summary of gas exchange field data normalized to a Schmidt number of 600 and plotted versus wind speed together with the empirical relationships of Liss and Merlivat [11] and ? (After Jähne and Haußecker [6])

A disadvantage of the CFT is that the transfer velocity of gases must be extrapolated from the transfer velocity of heat. The large difference in the Schmidt number (7 for heat, 600 for CO_2) casts some doubt whether the extrapolation to so much higher Schmidt numbers is valid.

Two variants of the technique proved to be successful. Active thermography uses a CO_2 laser to heat a spot of several centimeter in diameter on the water surface. The heat transfer rates are estimated from the temporal decay of the heated spot. Passive thermography uses the naturally occurring heat fluxes caused by latent heat flux j_l, sensible heat flux j_s and longwave emission of radiation j_r . The net heat flux $j_n = j_l + j_s + j_r$ results according to Eq. 8.4 in a temperature difference across the interface of $\Delta T = j_h/(\rho c_p k_h)$. Because of the turbulent nature of the exchange process any mean temperature difference is associated with surface temperature fluctuations which can be observed in thermal images. With this technique, the horizontal structure of the boundary layer turbulence can be observed. Surface renewal is directly observable in the IR image sequences, which show patches of fluid being drawn away from the surface.

With some knowledge about the statistics of the temperature fluctuations, the *temperature difference* ΔT across the interface as well as the time constant $\tilde{t}$ of heat transfer can be computed from the temperature distribution at the surface. Results obtained with this technique are shown in Fig. 8.4.

Summary of Field Data

A collection of field data is shown in Fig. 8.3. Although the data show a clear increase of the transfer velocity with wind speed, there is substantial scatter in the data that can only partly be attributed to uncertainties and systematic errors in the measurements.

Thus, in addition, the field measurements reflect the fact that the gas transfer velocity is not simply a function of the wind speed but depends significantly on other parameters influencing near-surface turbulence, such as the wind-wave field and the viscoelastic properties of the surface film.

Empiric Parametrization

Given the lack of knowledge, all theories about the enhancement of gas transfer by waves are rather speculative and are not yet useful for practical application. Thus, it is still state of the art to use semiempiric or empiric parameterizations of the gas exchange rate with the wind speed. Most widely used is the parametrization of Liss and Merlivat [11]. It identifies three physically well-defined regimes (smooth, wave-influenced, bubble-influenced) and proposes a piece-wise linear relation between the wind speed U and the transfer velocity k:

$$k = 10^{-6}\begin{cases} 0.472U(Sc/600)^{-2/3} & U \le 3.6\,\text{m/s} \\ 7.971(U-3.39)(Sc/600)^{-1.2} & U > 3.6\,\text{m/s and} \\ & U \le 13\,\text{m/s} \\ 16.39(U-8.36)(Sc/600)^{-1/2} & U > 13\,\text{m/s} \end{cases} \tag{8.16}$$

At the transition between the smooth and wavy regime, a sudden artificial jump in the Schmidt number exponent n from 2/3 to 1/2 occurs. This actually causes a discontinuity in the transfer rate for Schmidt number unequal to 600.

The empiric parametrization of Wanninkhof [25] simply assumes a quadratic increase of the gas transfer rate with the wind speed:

$$k = 0.861 \cdot 10^{-6}(s/m)U^2(Sc/600)^{-1/2}. \tag{8.17}$$

Thus, this model has a constant Schmidt number exponent n = 1/2. The two parameterizations differ significantly (see Fig. 8.3). The Wanninkhof parametrization predicts significantly higher values. The discrepancy between the two parameterizations and many others proposed (up to a factor of two) mirrors the current uncertainty in estimating the air-sea gas transfer rate.

Future Directions

In the past, progress toward a better understanding of the mechanisms of air–water gas exchange was hindered by inadequate measuring technology. However, new techniques have become available and will continue to become available that will give a direct insight into the mechanisms under both laboratory and field conditions.

This progress will be achieved by interdisciplinary research integrating such different research areas as oceanography, micrometeorology, hydrodynamics, physical chemistry, applied optics, and image processing.

Optical and image processing techniques will play a key role because only imaging techniques give direct insight to the processes in the viscous, heat, and mass boundary layers on both sides of the air–water interface. Eventually, all key parameters including flow fields, concentration fields, and waves will be captured by imaging techniques with sufficient spatial and temporal resolution. The experimental data gained with such techniques will stimulate new theoretical and modeling approaches.

Bibliography

Primary Literature

1. Bohr C (1899) Definition und methode zur bestimmung der invasions- und evasionscoefficienten bei der auflösung von gasen in flüssigkeiten. Werthe der genannten constanten sowie der absorptionscoefficienten der kohlensäure bei auflösung in wasser und in chlornatriumlösungen. Ann Phys Chem 68:500–525
2. Bolin B (1960) On the exchange of carbon dioxide between the atmosphere and the sea. Tellus 12(3):274–281. ISSN 2153-3490
3. Revelle R, Suess HE (1957) Carbon dioxide exchange between atmosphere and ocean and the question of an increase of atmospheric CO_2 during the past decades. Tellus 9:18–27
4. Jähne B (1982) Dry deposition of gases over water surfaces (gas exchange). In: Flothmann D (ed) Exchange of air pollutants at the air-earth interface (dry deposition). Battelle Institute, Frankfurt
5. Jähne B (2009) Air-sea gas exchange. In: Steele JH, Turekian KK, Thorpe SA (eds) Encyclopedia ocean sciences. Elsevier, Boston, pp 3434–3444
6. Jähne B, Haußecker H (1998) Air-water gas exchange. Annu Rev Fluid Mech 30:443–468
7. Reichardt H (1951) Vollständige darstellung der turbulenten geschwindigkeitsverteilung in glatten leitungen. Z Angew Math Mech 31:208–219
8. Peng TH, Broecker WS, Mathieu GG, Li Y-H, Bainbridge A (1979) Radon evasion rates in the Atlantic and Pacific oceans as determined during the geosecs program. J Geophys Res 84(C5):2471–2487
9. Roether W, Kromer B (1984) Optimum application of the radon deficit method to obtain air–sea gas exchange rates. In: Brutsaert W, Jirka GH (eds) Gas transfer at water surfaces. Reidel, Hingham, pp 447–457
10. Watson AJ, Upstill-Goddard RC, Liss PS (1991) Air-sea exchange in rough and stormy seas measured by a dual tracer technique. Nature 349(6305):145–147
11. Liss PS, Merlivat L (1986) Air-sea gas exchange rates: introduction and synthesis. In: Buat-Menard P (ed) The role of air-sea exchange in geochemical cycling. Reidel, Boston, pp 113–129
12. Deacon EL (1977) Gas transfer to and across an air-water interface. Tellus 29:363–374
13. Frew NM (1997) The role of organic films in air-sea gas exchange. In: Liss PS, Duce RA (eds) The sea surface and global change. Cambridge University Press, Cambridge, pp 121–171
14. Jacobs C, Nightingale P, Upstill-Goddard R, Kjeld JF, Larsen S, Oost W (2002) Comparison of the deliberate tracer method and eddy covariance measurements to determine the air/sea

transfer velocity of CO_2. In: Saltzman E, Donelan M, Drennan W, Wanninkhof R (eds) Gas transfer at water surfaces. Geophysical Monograph, vol 127. American Geophysical Union
15. Jähne B (1980) Zur Parametrisierung des Gasaustauschs mit Hilfe von Laborexperimenten. Dissertation, Institut für Umweltphysik, Fakultät für Physik und Astronomie, Univ. Heidelberg, http://d-nb.info/810123614. IUP D-145
16. Jähne B (1987) Image sequence analysis of complex physical objects: nonlinear small scale water surface waves. In: Proceedings of 1st international conference on computer vision, London, pp 191–200
17. Jähne B (1991) New experimental results on the parameters influencing air-sea gas exchange. In: Wilhelms SC, Gulliver JS (eds) Air-water mass transfer, Selected papers from the 2nd international symposium on gas transfer at water surfaces, Minneapolis, 11–14 Sep 1990. ASCE, pp 582–592
18. Jähne B, Heinz G, Dietrich W (1987) Measurement of the diffusion coefficients of sparingly soluble gases in water. J Geophys Res 92(C10):10,767–10,776
19. Keeling RF (1993) On the role of large bubbles in air-sea gas exchange and supersaturation in the ocean. J Marine Res 51:237–271
20. King DB, Bryun WJD, Zheng M, Saltzman ES (1995) Uncertainties in the molecular diffusion coefficient of gases in water for use in the estimation of air-sea exchange. In: Jähne B, Monahan E (eds) Air-water gas transfer, Selected papers, 3rd international symposium on air-water gas transfer. AEON, Hanau, pp 13–22
21. McKenna SP, Bock EJ (2006) Physicochemical effects of the marine microlayer on air-sea gas transport. In Gade M, Hühnerfuss H, Korenowski GM (eds) Marine surface films: chemical characteristics, influence on air-sea interactions, and remote sensing. Springer, Berlin/ Heidelberg, pp 77–91
22. Sündermann J (ed) (1986) Landolt-Börnstein, vol V 3c, Oceanography. Springer, Heidelberg
23. Torgersen T, Top Z, Clarke WB, Jenkins WJ (1977) A new method for physical limnology-tritium-helium-3 ages results for Lakes Erie, Huron, and Ontario. Limnol Oceanogr 22:181–193
24. Tschiersch J, Jähne B (1980) Gas Exchange trough a rough water surface in a circular windtunnel; Wave characteristics under limited and unlimited fetch. In: Broecker HC, Hasse L (eds) Berichte aus dem Sonderforschungsbereich 94 Meeresforschung – Symposium on capillary waves and gas exchange, Trier, 2–6 July 1979, number 17. Univ. Hamburg, pp 63–70
25. Wanninkhof R (1992) Relationship between wind speed and gas exchange over the ocean. J Geophys Res 97:7373–7382
26. Woolf D, Leifer I, Nightingale P, Rhee T, Bowyer P, Caulliez G, de Leeuw G, Larsen S, Liddicoat M, Baker J, Andreae M (2007) Modelling of bubble-mediated gas transfer: fundamental principles and a laboratory test. J Marine Syst 66:71–91

Books and Reviews

Banner ML (ed) (1999) The wind-driven air-sea interface, electromagnetic and acoustic sensing, wave dynamics and turbulent fluxes, proceedings of the symposium Sydney, Australia, 11–15 January 1999. University of New South Wales, Sydney

Bengtsson LO, Hammer CU (eds) (2001) Geosphere-biosphere interactions and climate. Cambridge University Press, Cambridge

Borges AV, Wanninkhof R (2007) Fifth international symposium on gas transfer at water surfaces. J Mar Syst 66(1–4):1–308

Brasseur GP, Prinn RG, Pszenny AA (eds) (2003) Atmospheric chemistry in a changing world. An integration and synthesis of a decade of tropospheric chemistry research. Springer, Berlin

Brutsaert W, Jirka GH (eds) (1984) Gas transfer at water surfaces. Reidel, Dordrecht

Csanady GT (2001) Air-sea interaction, laws and mechanisms. Cambridge University Press, Cambridge
Cussler EL (2009) Diffusion – mass transfer in fluid systems, 3rd edn. Cambridge University Press, Cambridge
Danckwerts PV (1970) Gas-liquid reactions. MacGraw-Hill, New York
Davies JT (1972) Turbulence phenomena. An introduction to the eddy transfer of momentum, mass, and heat, particularly at interfaces. Academic, New York/London
Davies JT, Rideal EK (1963) Interfacial phenomena, 2nd edn. Acadamic, New York
Dobson F, Hasse L, Davis R (eds) (1980) Air-sea interaction: instruments and methods. Plenum, New York
Donelan MA, Hui WH, Plant WJ (eds) (1996) The air-sea interface, radio and acoustic sensing, turbulence and wave dynamics, proceedings of the symposium, Marseille, France, 24–30 June 1993. Rosenstiel School of Marine and Atmospheric Science, University of Miami, Miami, Florida
Donelan MA, Drennan WM, Saltzman ES, Wanninkhof R (eds) (2002) Gas transfer at water surfaces. American Geophysical Union, Washington, DC
Emerson SR, Hedges J (2008) Chemical oceanography and the marine carbon cycle. Cambridge University Press, Cambridge
Favre A, Hasselmann K (eds) (1978) Turbulent fluxes through the sea surface, wave dynamics, and prediction, proceedings of the symposium, Marseille, 1977. Plenum, New York
Fogg PGT, Sangster J (2003) Chemicals in the atmosphere: solubility, sources, and reactivity. Wiley, Chichester
Gade M, Hühnerfuss H, Korenowski GM (eds) (2005) Marine surface films: chemical characteristics, influence on air-sea interactions and remote sensing. Springer, Berlin
Garbe CS, Handler RA, Jähne B (eds) (2007) Transport at the air sea interface – measurements, models and parameterizations. Springer, Berlin
Gulliver JS (2007) Introduction to chemical transport in the environment. Cambridge University Press, Cambridge
Jähne B, Monahan EC (eds) (1995) Air-water gas transfer – selected papers from the third international symposium on air-water gas transfer. AEON Verlag & Studio Hanau. http://d-nb.info/946682526
Kantha LH, Clayson CA (2000) Small scale processes in geophysical fluid flows, vol 67, International geophysics series. Acadamic, San Diego
Komori S, McGillis W (eds) (2011) Gas transfer at water surfaces, selected papers from the 6th international symposium. Kyoto University Press, Kyoto
Kraus EB, Businger JA (1994) Atmosphere-ocean interaction, vol 27, 2nd edn, Oxford monographs on geology and geophysics. Oxford University Press, New York
Liss PS, Duce RA (eds) (2005) The sea surface and global change. Cambridge University Press, Cambridge
Robinson IS (2010) Discovering the ocean from space – the unique applications of satellite oceanography. Springer, Heidelberg
Sarmiento JL, Gruber N (2006) Ocean biogeochemical dynamics. Princeton University Press, Princeton
Soloviev A, Lukas R (2006) The near-surface layer of the ocean, vol 31, Atmospheric and oceanographic sciences library. Springer, Dordrecht
Wanninkhof R, Asher WE, Ho DT, Sweeney C, McGillis WR (2009) Advances in quantifying air-sea gas exchange and environmental forcing. Annu Rev Mar Sci 1:213–244
Wilhelms SC, Gulliver JS (eds) (1991) Air-water mass transfer – selected papers from the 2nd international symposium on gas transfer at water surfaces, Minneapolis Minnesota, September 11–14, 1990. American Society of Civil Engineers, New York
Zeebe RE, Wolf-Gladrow DA (2001) CO_2 in seawater: equilibrium, kinetics, isotopes, vol 65, Elsevier oceanography series. Elsevier, Amsterdam